Toward Higher Nuclearity: Tetranuclear Cobalt(II) Metallogrid Exhibiting Spin Crossover

ARTICLE *in* INORGANIC CHEMISTRY · FEBRUARY 2014

Impact Factor: 4.76 · DOI: 10.1021/ic402971a · Source: PubMed

4 AUTHORS, INCLUDING:

Shu-Qi Wu
Kyushu University
10 PUBLICATIONS **67** CITATIONS

SEE PROFILE

Inorganic Chemistry

Article

pubs.acs.org/IC

Toward Higher Nuclearity: Tetranuclear Cobalt(II) Metallogrid Exhibiting Spin Crossover

Shu-Qi Wu, Yi-Tong Wang, Ai-Li Cui, and Hui-Zhong Kou*

Department of Chemistry, Tsinghua University, Beijing 100084, People's Republic of China

Supporting Information

ABSTRACT: Supramolecular strategy was employed to achieve the highest nuclearity Co(II) cluster exhibiting spin-crossover (SCO) behavior. Magnetic susceptibility characterization of the Co_4^{II} complex shows that two different spin-transition processes occur. The SCO behavior is directed by the partially deprotonated polydentate ligand, which favors the structural distortion required by the spin transition.

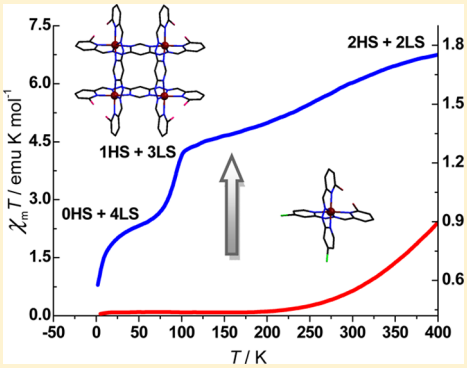

1. INTRODUCTION

Bistability phenomenon is of vital importance in the development of molecular-based devices, especially in the field of high-density information storage and molecular electronics. Spin-crossover (SCO) complexes exhibiting spin transition between two stable spin states, that is, the low-spin state (LS) and the high-spin state (HS), under relatively minor external stimuli such as temperature, pressure, or light have potential applications in designing molecular switches and memory devices.[1,2]

It is generally recognized that complexes with abrupt spin-transition process and temperature hysteresis loops are most likely to be applied into memory devices or chemosensors.[3] Theoretically, strong interaction between metal centers would probably result in higher cooperativity and hence a greater chance to achieve desired properties.[3,4g] As a result, to enhance the interaction between metal ions via superexchange and/or intramolecular interaction remains attractive among researchers. In this context, the polynuclear strategy has emerged,[5−14] and some polynuclear clusters and extended one-dimensional (1D), two-dimensional (2D), and three-dimensional (3D) frameworks are found to exhibit more versatile magnetic properties, for example, multistep SCO via nonsimultaneous spin-transition process[14a] and active guest-tuned SCO behavior.[5b]

As a family of well-assembled polynuclear complexes, metallogrid complexes[9c] stand out in the field of magnetochemistry due to their tunable magnetic performances dictated by rational selection of linkers and regular geometric structures applicable to certain surfaces.[9a,b] The past decade has witnessed progressive prosperity since Lehn and his co-workers first introduced SCO phenomenon to the Fe_4 grid complexes.[12,13] Up to now, several Fe_4 grid complexes have been reported, some of which display interesting multistep SCO and light-induced excited-spin-state trapping (LIESST).[12,14]

However, compared with various Fe^{II} SCO complexes, Co^{II} SCO complexes are still limited, not to mention polynuclear ones.[3,7,15] The reported highest nuclearity SCO Co^{II} cluster was achieved in a family of tricobalt molecular wires.[7] Rational design of polynuclear SCO Co^{II} complexes remains a challenge.

SCO behavior is observed in a newly synthesized mononuclear Co^{II} complex, $[Co(L^1)_2]\cdot 0.5DMF$ (**1**), (DMF = dimethylformamide) obtained through the reaction of HL^1 (HL^1 = 4-(2-((6-bromopyridin-2-yl)methylene)hydrazinyl)-6-chloropyrimidine) (Scheme 1) and $Co(ClO_4)_2\cdot 6H_2O$. Enlightened by this discovery, we used the hexadentate ligand H_2L^3 (H_2L^3 = 4,6-bis(2-((6-bromopyridin-2-yl)methylene)-hydrazinyl)pyrimidine) to react with cobalt salts because the ligand tends to form gridlike metallic complexes.[9a] It was hoped that weak magnetic interaction via pyrimidine bridges would not damage the SCO behavior while enhancing the cooperativity.[16] A gridlike cobalt(II) complex, $[Co_4(HL^3)_4]$-

Scheme 1. Ligands Used in This Work

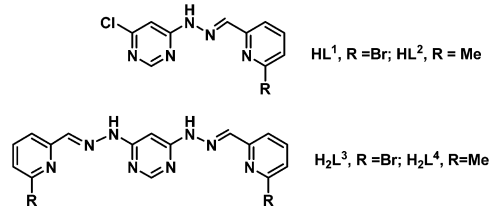

Received: December 3, 2013
Published: February 20, 2014

   dx.doi.org/10.1021/ic402971a | Inorg. Chem. 2014, 53, 2613−2618

$(ClO_4)_4·8H_2O$ (**3**), was obtained. Interestingly, complex **3** shows two different spin-transition processes. One of these is abrupt, while the other one is gradual. Complex **3** is by far the highest nuclearity Co^{II} cluster with SCO behavior. By changing the substituent groups of the ligands from Br to CH_3, two Co^{III} complexes, $[Co(L^2)_2]ClO_4$ (**2**) and $[Co_4(L^4)_4](ClO_4)_4·16H_2O$ (**4**), were obtained (Scheme 1).

2. RESULTS AND DISCUSSION

Complexes **1** and **2** were prepared by reacting $HL^{1,2}$ with $Co(ClO_4)_2·6H_2O$ in MeOH. Single crystals of complexes **3** and **4** were obtained by slow diffusion of an aqueous solution of $NaClO_4$ into the methanol solution of $H_2L^{3,4}$ and $CoCl_2·6H_2O$. The electrospray mass spectrum of complex **3** in MeOH shows peaks for species $[Co_4(HL^3)(L^3)_3]^+$ (m/z = 2133.19), $[Co_4(HL^3)_2(L^3)_2]^{2+}$ (m/z = 1066.73), $[Co_4(HL^3)_3(L^3)]^{3+}$ (m/z = 711.49), and $(H_2L^3 + H)^+$ (m/z = 477.03), indicating that tetranuclear Co^{II} grids formed in MeOH (Figure S1, Supporting Information). The ultraviolet−visible (UV−vis) spectra of complexes **1** and **3** in a methanol−DMF mixture show broad and intense absorptions at 443 and 530 nm, respectively (Figure S2, Supporting Information). The bands should be assigned to $\pi-\pi^*$ absorption of the ligands. The conjugation of the H_2L^3 compared with that of HL^1 is responsible for the red shift of the band. The d−d transitions have been obscured by the broad $\pi-\pi^*$ bands.

2.1. Crystal Structures. Crystallographic data of complexes **1**−**4** at different temperatures are listed in Table 1. Comparisons of Co−N bond lengths (Å) and structural distortion parameters for complexes **1**−**4** are collected in Tables 2 and 3.

Structural determination shows that complexes **1** and **2** share a similar coordination mode. Two perpendicular deprotonated ligands chelated Co ions to form $[Co(L^x)_2]^{0/+1}$ core (Figure 1 and Figure S5 of the Supporting Information). For complex **1**, each tridentate ligand coordinates Co^{II} ion equatorially, via four pyridyl and pyrimidyl donors, and axially, via two imine N atoms (abbreviated as N_{py}, N_{pym}, and N_{imi}, respectively), to complete the coordination sphere. The length of the axial Co−N_{imi} bond (1.875−1.895 Å) is evidently shorter than that of the Co−N_{py} and Co−N_{pym} bonds (1.998−2.222 Å) at 123 K, forming a compressed octahedral coordination sphere due to significant Jahn−Teller distortion of LS Co^{II} ion.[4d] The bond distortion parameter Δ decreases while the angular distortion parameters increase upon heating process (Table 2), suggestive of the partial disappearance of the Jahn−Teller distortion due to occurrence of spin-transition process.[4h,17] The molecules are well-separated with the $Co^{II}\cdots Co^{II}$ separation of 8.951 Å at 123 K. The Cl···Cl interaction (3.277 Å at 123 K) leads to the formation of a supramolecular dimer (Figure S6, Supporting Information). The Co−N bond length in complex **2** ranges from 1.876 Å to 2.018 Å, with an average Co−N bond distance of 1.940 Å, consistent with the Co^{III} ions supported further by the Bond Valence Sum (BVS) results[4h] and the relatively smaller structural distortion parameters (Table 3) due to the t_{2g}^6 electronic configuration.[18]

Complexes **3** and **4** share a similar $[Co_4]^{4+}$ core structure with different deprotonated ligands (Figures 1 and Figure S7 of the Supporting Information). For complex **3**, the Co_4 grid core is composed of four partially deprotonated ligands $(HL^3)^-$ and four octahedral Co^{II} ions. The high symmetry yields only one crystallographically independent Co ion. The adjacent Co···Co distance is 6.175 Å, and diagonal Co ions are separated by

Table 1. Crystallographic Data of Complexes 1−4

	1·123 K	**1**·298 K	**2**·298 K	**3**·153 K	**3**·253 K	**4**·153 K
formula	$C_{21.3}H_{15.5}N_{10.5}O_{0.3}Br_2Cl_2Co$	$C_{21.3}H_{15.5}N_{10.5}O_{0.5}Br_2Cl_2Co$	$C_{22}H_{18}N_{10}O_4Cl_3Co$	$C_{64}H_{60}N_{32}O_{24}Br_8Cl_4Co_4$	$C_{64}H_{60}N_{32}O_{24}Br_8Cl_4Co_4$	$C_{72}H_{96}Cl_4Co_4N_{32}O_{32}$
Fw	718.59	718.59	651.74	2678.14	2678.14	2299.27
crystal system	monoclinic	monoclinic	monoclinic	tetragonal	tetragonal	tetragonal
space group	$C2/c$	$C2/c$	$P2(1)/c$	$P4(2)/nmc$	$P4(2)/nmc$	$I4(1)/a$
a (Å)	29.4329(13)	29.3456(15)	8.9811(10)	22.639(3)	22.615(3)	17.276(2)
b (Å)	12.9537(7)	13.0477(7)	16.9120(17)	22.639(3)	22.615(3)	17.276(2)
c (Å)	14.6693(7)	14.8443(10)	17.1719(19)	12.961(3)	13.039(4)	30.908(5)
B (deg)	114.9420(13)	114.6280(15)	95.615(3)	90	90	90
V (Å^3)	5071.3(4)	5166.7(5)	2595.7(5)	6642.8(19)	6669(4)	9224.6(1)
Z	8	8	4	2	2	4
ρ_{calcd} (g cm^{-3})	1.882	1.848	1.668	1.472	1.466	1.656
μ (mm^{-1})	4.077	4.002	1.022	3.050	3.038	0.924
GOF	1.003	1.069	1.100	1.134	1.124	1.156
$R1$ [$I > 2\sigma(I)$]	0.0362	0.0534	0.0586	0.0871	0.0806	0.0745
$wR2$ (all data)	0.0945	0.1974	0.1785	0.2623	0.2296	0.1863

dx.doi.org/10.1021/ic402971a | Inorg. Chem. 2014, 53, 2613−2618

Table 2. Comparisons of Co−N Bond Lengths (Å) And Structural Distortion Parameters for Complexes 1 and 3

	1·123 K	1·298 K	3·153 K	3·253 K
$Co-N_{py}$	2.147(2), 2.222(2)	2.166(4), 2.213(4)	2.196(5)	2.205(5)
$Co-N_{imi}$	1.875(2), 1.895(2)	1.895(4), 1.904(4)	2.051(6)	2.061(5)
$Co-N_{pym}$	2.055(2), 1.998(2)	2.055(5), 2.010(4)	2.109(5)	2.130(5)
$Co-N_{av}$	2.032(2)	2.041(4)	2.119(5)	2.132(5)
Σ (deg)[4h,17]	98.9	102.1	133.0	134.1
θ (deg)[4h,17]	173.5	177.8	222.2	223.3
dihedral angle (deg)	89.5	89.4	84.1	84.6
Δ[4h,17]	3.8×10^{-3}	3.5×10^{-3}	7.9×10^{-4}	7.6×10^{-4}
BVS[a]	2.32	2.26	1.76	1.70

[a]The BVS values are calculated based on a R_0 value of 1.66 Å for Co(II)−O and Co−N.[4h]

Table 3. Comparisons of Co−N Bond Lengths (Å) And Structural Distortion Parameters for Complexes 2 and 4

	2·298 K	4·153 K
$Co-N_{py}$	2.017(3), 2.018(3)	1.991(3), 1.992(3)
$Co-N_{imi}$	1.876(3), 1.880(3)	1.881(3), 1.883(3)
$Co-N_{pym}$	1.928(3), 1.921(3)	1.932(3), 1.934(3)
$Co-N_{av}$	1.940(3)	1.936(3)
Σ (deg)[4h,17]	71.4	72.5
θ (deg)[4h,17]	124.4	123.5
dihedral angle (deg)	89.7	89.3
Δ[4h,17]	9.0×10^{-4}	5.3×10^{-4}
BVS[4h]	2.85	2.87

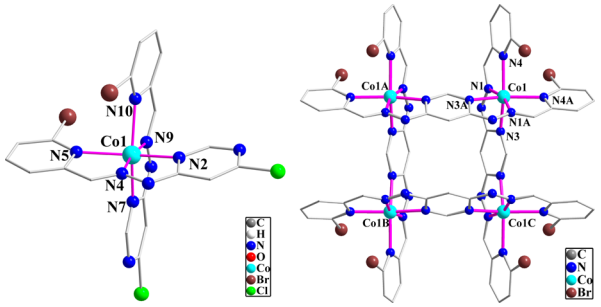

Figure 1. Crystal structure of complexes (left) **1** and (right) **3**. Hydrogen atoms, anions, and solvents have been omitted for clarity.

8.731 Å at 153 K within a grid molecule. The four Co^{II} ions in the grid are perfectly coplanar, and two ligands lie above the Co_4 plane and the others below. Each Co^{II} ion is coordinated by six nitrogen atoms from two nearly perpendicular ligands with a dihedral angle of 84.1° at 153 K (84.6° at 253 K), evidently smaller than those of complexes **1** and **4**. This distortion may be caused by the competition between the Jahn−Teller effect of the LS Co^{II} ion and the thermodynamic trend to form a regular gridlike Co_4 cluster. The average Co−N bond distance of 2.119(5) Å indicates the presence of HS Co^{II} ions at 153 K, comparable to the reported mononuclear SCO complexes.[4,19] The axial $Co-N_{imi}$ bond distances (2.057 Å) are apparently shorter than those of the equatorial Co−N bonds (2.102−2.197 Å), affording an axially compressed octahedral geometry of the Co^{II} ion. This structural distortion should be ascribed to the Jahn−Teller effect for the LS Co^{II} ions with the electronic configuration of $t_{2g}^6e_g^1$, suggestive of the presence of some LS Co^{II} ions at 153 K. Therefore, the Co−N bond distance should be taken as the average values of LS Co^{II} and HS Co^{II} ions. Like complex **1**, the bond distortion parameter Δ decreases while the angular distortion parameters increase with rising temperature (Table 2), indicating the occurrence of spin transition. For complex **4**, four doubly deprotonated ligands $(L^4)^{2-}$ and four Co^{III} ions form the cationic grid. The Co−N bond lengths range from 1.879 Å to 2.009 Å with an average distance of 1.936 Å and small octahedral distortion parameters (Table 3), consistent with the Co^{III} ions with the electronic configuration of t_{2g}^6.[18]

The packing of complexes **3** and **4** was mainly directed by the Br···Br contacts, H bonds, and other intermolecular bonds, yielding a regular 3D packing network. The water and perchlorate ions are incorporated in the formed cavities. The Br···Br contacts for the adjacent ligand in the molecule are 3.533 Å, connecting the adjacent Co_4 molecules into a 3D framework (Figure S8, Supporting Information).

2.2. Magnetic Properties. The direct-current magnetic susceptibility measurement of complex **1** was performed in the range of 5−400 K under 1000 Oe external field (Figure 2).

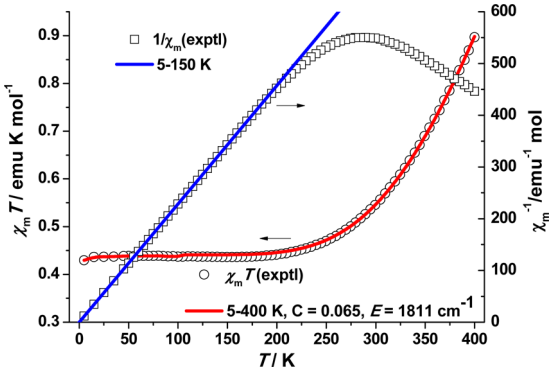

Figure 2. Temperature dependence of $\chi_m T$ for complex **1**, and Curie−Weiss fitting of reciprocal susceptibility.

Complex **1** was stable enough during the warming process, as supported by TGA analysis (Supporting Information). The $\chi_m T$ value decreases gradually from 0.900 emu K mol^{-1} at 400 K to a plateau below 200 K. Magnetic susceptibility data in the range of 5−150 K obey the Curie−Weiss law, with the Curie constant of 0.437 emu K mol^{-1}. Theoretically, the LS Co^{II} ion gives a spin-only $\chi_m T$ value of 0.375 emu K mol^{-1} ($S = 1/2$ with an isotropic g value of 2.0). The small deviation should be ascribed to Jahn−Teller distortion of the ^2E ground spin state. The isotropic g value obtained from Curie−Weiss fitting is 2.15, comparable with the reported LS Co^{II} complexes.[4j] Reciprocal magnetic susceptibility at higher temperature evidently deviates from a straight line due to the spin transition. The energy separation between the LS ^2E state and the HS $^4T_1$ state is obtained as 1811 cm^{-1} by fitting the susceptibility data in the

dx.doi.org/10.1021/ic402971a | Inorg. Chem. 2014, 53, 2613−2618

whole temperature range to a model proposed by Harris et al.[4i] The ratio of the vibrational partition function of the LS to that of the HS state is given as 0.065, suggestive of the more favorable LS state. These parameters are very similar to those of the SCO complex $[Co(terpy)_2]Cl_2$ (terpy = 2,2′:6′,2″-terpyridine).[4i,j]

The electron paramagnetic resonance (EPR) spectra of complex **1** at 100 K give two anisotropic signals, corresponding to $g_{\parallel} = 2.11$ and $g_{\perp} = 2.07$ (inset of Figure 3). The isotropic g value can be calculated as $g_{iso} = (g_{\parallel} + 2g_{\perp})/3 = 2.08$, typical of $S = 1/2$ LS Co^{II} species.[4j] The amount of HS Co^{II} increases with increasing temperature, which results in the broadening of the EPR peaks. The experimental $\chi_m T$ value at room temperature is mostly in the range of 2.7−3.4 emu K mol^{-1} for high-spin Co^{II} complexes due to the orbital contribution.[20] The small $\chi_m T$ value of 0.54 emu K mol^{-1} at room temperature indicates that the amount of HS Co^{II} is very low. No EPR signal can be observed at 298 K; however, a broad isotropic signal centered at $g = 2.07$ was observed in a diluted DMF solution at 298 K. Hence this phenomenon is related to the fast-spin relaxation process in crystalline samples.[4n]

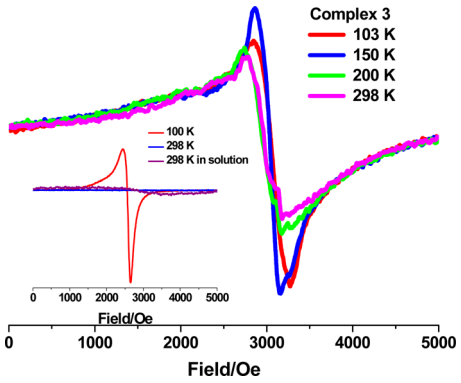

Figure 3. EPR spectra at different temperatures for complexes **3** and (inset) **1**.

The magnetic susceptibility measurement of complex **3** reveals an intriguing stepwise SCO behavior in the temperature range from 2 to 400 K (Figure 4). Complex **3** was not that stable during the warming process, but its magnetic properties stay nearly unchanged, corroborated by magnetic susceptibility analyses (Figure S9, Supporting Information). It has been shown that the magnetic coupling through the pyrimidine bridge is weak; thus, the complex should be treated as four weakly coupled Co^{II} ions.[16] The $\chi_m T$ value at 400 K is approximately 6.75 emu K mol^{-1}, gradually decreasing to 4.46 emu K mol^{-1} at 130 K. Below 100 K, the $\chi_m T$ value decreases suddenly from 4.16 to 2.57 emu K mol^{-1} at 70 K and then reaches a small plateau. The $\chi_m T$ decreases further upon cooling, reaching 0.79 emu K mol^{-1} at 2 K. The Co_4^{II} cluster could be deduced to four independent Co^{II} ions when the magnetic coupling is negligibly small. The content of the LS Co^{II} ions can be estimated by using the $\chi_m T$ value of 3.0 emu K mol^{-1} for HS Co^{II} and 0.4 emu K mol^{-1} for LS Co^{II}.[20] The $\chi_m T$ value of 6.75 emu K mol^{-1} at 400 K confirms the presence of ca. 50% low-spin Co^{II} ions, that is, 2HS + 2LS in a molecule. The nearly linear decrease of $\chi_m T$ from 400 to 130 K should be due to a gradual SCO of Co^{II} ions rather than to the spin−orbital coupling contribution. The decrease of $\chi_m T$ by 2.3 emu K mol^{-1} corresponds approximately to the spin transition of one Co^{II} ion, and therefore the spin state at 130 K becomes 1HS + 3LS. The abrupt decrease by 2.0 emu K mol^{-1} from 130 to 70 K can be ascribed to the abrupt SCO of the remaining HS Co^{II} ion. Therefore, complex **1** undergoes a two-step spin transition, one abrupt and the other gradual. Heating−cooling cycles in the temperature range of 5−400 K indicate that no hysteresis occurs in both spin-transition processes (Figure S5, Supporting Information). The further decrease of $\chi_m T$ below 50 K should be ascribed to the antiferromagnetic coupling between the adjacent Co^{II} ions and/or to the zero-field splitting (ZFS) effect of the remaining HS Co^{II} in the Co_4 molecule.

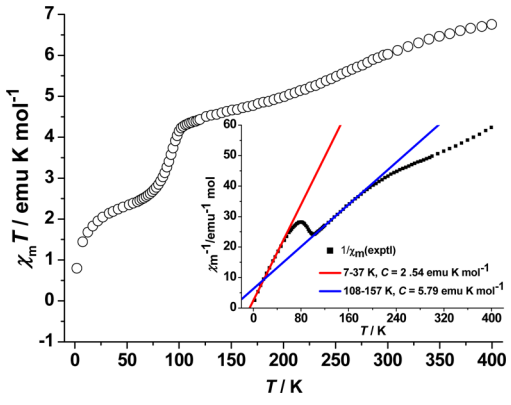

Figure 4. Temperature dependence of $\chi_m T$ per Co_4 for complex **3**. Inset: Curie−Weiss fitting of reciprocal susceptibility.

The reciprocal magnetic susceptibility versus temperature curve evidently deviates from a straight line (inset of Figure 4), and the two-step spin-transition process becomes more obvious, as anticipated for SCO complexes. Magnetic susceptibility data between 7 and 37 K and 108−157 K are fitted by the Curie−Weiss law to partly take into account ZFS and weak magnetic coupling. The resulting Curie constants of these two temperature ranges are 2.55 and 5.79 emu K mol^{-1}, respectively. It is worth noting that the Curie constant of 7−37 K is apparently larger than the theoretical $\chi_m T$ value for four LS Co^{II} ions (∼1.6 emu K mol^{-1}), which indicates the presence of small quantities of HS Co^{II} ions (estimated as 0.36 HS Co^{II} ions versus 3.64 LS Co^{II} ions). The Curie constant of 108−157 K yields 1.61 HS Co^{II} ions versus 2.39 LS Co^{II} ions, further confirming the spin transition of a single Co^{II} ion.

The EPR spectra of complex **3** in the range of 103−298 K exhibit two anisotropic signals around 2.0, typical of the LS Co^{II} ion in the compressed octahedral ligand field (Figure 3). The isotropic g value obtained from experimental data are 2.17 (103 K), 2.19 (150 K), 2.25 (200 K), and 2.23 (298 K), typical of the LS Co^{II} ion. The signals broaden, and the peak heights decline, originating from the decline of the ratio of LS Co^{II} ions as well as the temperature effect.

Complexes **2** and **4** are temperature-independent paramagnetic (TIP), corresponding to the LS Co^{III} ions. It is interesting to find a ligand-dependent control over the valence of the cobalt ions in this series of complexes. Considering complexes **1**, **2**, and **4**, the electronic effect rather than the basicity of the $(L^2)^-$ and $(L^4)^{2-}$ ligands is responsible for the higher oxidation state of cobalt ions in complexes **2** and **4**. The weak electronic donating effect of the methyl group, compared with the bromide atom that is recognized to possess neutral electronic effect or weak electron-withdrawing effect, would increase the negative electronic density of N atom from pyridine (N_{py}). This assertion is supported by the density

dx.doi.org/10.1021/ic402971a | Inorg. Chem. 2014, 53, 2613−2618

functional theory (DFT) calculation (see computational details, Supporting Information) of $(L^1)^-$ and $(L^2)^-$. The N_{py} atom of $(L^2)^-$ possesses 0.16 negative charges more than that of $(L^1)^-$, which tends to stabilize the higher oxidation state of cobalt ions.

Though a few gridlike Co^{II} complexes have been reported, most of them show the magnetism of antiferromagnetic coupled HS Co^{II} ions.[21] To fine-tune the strength of the ligand field is an effective strategy. In our Work, the deprotonated ligand $(HL^3)^-$ provides a compressed octahedral coordination sphere to stabilize the LS Co^{II} ions, and the weak electronic effect of the substituent group of the pyridine ring adjusts the electronic density and hence the strength of the ligand field. Furthermore, the substituent group of the pyridine ring rather than that of the pyrimidine ring would play a more important role in steric hindrance effect.[21] It is worth noting that compared with that of complex **1**, the spin-transition process of complex **3** can occur at lower temperatures, in accordance with the fact that a partially deprotonated ligand weakens its ligand field.

3. CONCLUSION

In conclusion, two-step SCO has been for the first time observed in a gridlike Co_4^{II} complex. The SCO in the tetranuclear complex is directed by the partially deprotonated polydentate ligand, which favors the structural distortion required by the spin transition. The present Work illustrates that the strategy utilizing the Jahn−Teller effect, the electronic effect, and the steric hindrance effect should open a new avenue for the design of new Co^{II} SCO complexes. Future work along this line of consideration is in progress in our laboratory.

4. EXPERIMENTAL SECTION

IR spectra were recorded on a Nicolet Magna-IR 750 spectrometer in the 4000−650 cm^{-1} region. Elemental analyses (C, H, N) were performed on an Elementar Vario MICRO CUBE analyzer. ESI-MS spectra were performed on ThermoFisher LTQ Orbitrap XL. Temperature- and field-dependent magnetic susceptibility measurements were carried out on a Quantum Design SQUID magnetometer. Well-shaped single crystals were collected and used for magnetic measurements. The experimental susceptibilities were corrected for the diamagnetism of the constituent atoms (Pascal's tables).

Single-crystal X-ray data were collected on a Rigaku Saturn724+ CCD or a Rigaku R-AXIS RAPID IP diffractometer. The structures were solved by direct method (SHELXS-97) and refined by full-matrix least-squares (SHELXL-97)[22] on F^2. Anisotropic thermal parameters were used for the non-hydrogen atoms and isotropic parameters for the hydrogen atoms. Hydrogen atoms were added geometrically and refined using a riding model.[22] Because of the weak diffraction and/or disordered solvents, the solvent molecules cannot be exactly modeled. The SQUEEZE function of PLATON was applied[23] and gave available voids of 2879.5 $Å^3$ and 2910.1 $Å^3$ for complex **3**·153 K and **3**·253 K, respectively. The corresponding residual electron counts were 631 e^- and 791 e^- per unit cell, corresponding to the missing solvent molecules.

4.1. Synthesis of 4-Chloro-6-hydrazinylpyrimidine. Hydrazine hydrate (80%) (30 mL) was cooled to −10 °C, and solid 4,6-dichloropyrimidine (7.50 g, 50 mmol) was slowly added in. The mixture was stirred rigorously until it turned pale yellow. The mixture was further stirred under room temperature for 4 h, and then the solid was filtered off. The filtrate was washed with water and methanol and then dried under vacuum. The product yield was about 60%. IR (KBr, cm^{-1}): 3235, 2033, 1638, 1618, 1573, 1397, 1080. Elemental analysis (%) for $C_4H_5N_4Cl$, calculated: C 33.23, N 38.76, H 3.49; found: C 33.52, N 38.90, H 4.00.

4.2. Synthesis of the Ligand $HL^{1,2}$. A mixture of 4-chloro-6-hydrazinylpyrimidine (2.90 g, 20 mmol) and 6-bromo-pyridylaldehyde (3.8 g, 20 mmol) was stirred in 30 mL of ethanol for 1 h. The precipitate was obtained after it was filtered off, washed with ethanol and diethyl ether, and dried. The product yield of HL^1 was about 80%. IR (KBr, cm^{-1}): 3253, 2033, 1630, 1132. Elemental analysis (%) for $C_{10}H_7N_5BrCl$, calculated: C 38.43, N 22.41, H 2.26; found: C 38.68, N 22.34, H 2.81.

Ligand HL^2 (HL^2 = 4-chloro-6-(2-((6-methylpyridin-2-yl)-methylene)hydrazinyl)pyrimidine) was synthesized with a procedure similar to that used for preparing HL^1, using 6-methyl-pyridylaldehyde instead of 6-bromo-pyridylaldehyde. IR (KBr, cm^{-1}): 3237, 2819, 1638, 1618, 1560, 1442, 1372.

4.3. Synthesis of the Ligand $H_2L^{3,4}$. 2,4-dihydrazinopyrimidine was synthesized following the literature method.[24] A mixture of 2,4-dihydrazinopyrimidine (2.80 g, 20 mmol) and 6-bromo-pyridylaldehyde (7.6 g, 40 mmol) was stirred in 30 mL of ethanol for 30 min. The precipitate was obtained after it was filtered off, washed with ethanol and diethyl ether, and dried. The product yield of H_2L^3 was nearly 100%. Ligand H_2L^4 (H_2L^4 = 4,6-bis(2-((6-methylpyridin-2-yl)-methylene)hydrazinyl)pyrimidine) was synthesized with a procedure similar to that used for preparing H_2L^3, using 6-methyl-pyridylaldehyde instead of 6-bromo-pyridylaldehyde.

4.4. Synthesis of $Co^{II}(L^1)_2$·0.5DMF (1) and $[Co^{III}(L^2)_2]ClO_4$ (2). HL^1 (0.1 mmol) and $Co(ClO_4)$·$6H_2O$ (0.1 mmol) were dissolved in MeOH (15 mL) and stirred under room temperature for 20 min. The collected precipitate was dissolved in MeOH−DMF. Slow evaporation of the resulting solution for 3 d gave brown single block-like crystals of complex **1** suitable for structural analysis. Yield: 70%. IR (KBr, cm^{-1}): 2030, 1776, 1626, 1384. Complex **2** was obtained by a procedure similar to that used for preparing complex **1**, except HL^2 was employed instead of HL^1. The product yield of **2** was 60%. IR (KBr, cm^{-1}): 2032, 1622, 1548, 1456, 1218, 1102.

4.5. Synthesis of $[Co_4^{II}(HL^3)_4](ClO_4)_4$·$8H_2O$ (3) and $[Co^{III}_4(L^4)_4]$-$(ClO_4)_4$·$16H_2O$ (4). H_2L^3 (0.1 mmol) and $CoCl_2$·$6H_2O$ (0.1 mmol) were dissolved in MeOH (15 mL) and stirred under room temperature for 3 h. The suspension was then filtered, and the solution was diffused with an aqueous solution of $NaClO_4$ in a single glass tube. Dark brown block-like single crystals of complex **3** suitable for structural analysis were obtained after 2 weeks. Yield: 40%. Elemental analysis (%) for $C_{64}H_{60}N_{32}Br_8Cl_4O_{24}Co_4$, calculated: C 28.70, N 16.74, H 2.26; found: C 28.88, N 16.77, H 2.24. IR (KBr, cm^{-1}): 1633, 1537, 1441, 1188, 1100. Complex **4** was prepared by using a procedure similar to that of complex **3** except the employment of H_2L^4 instead of H_2L^3. Dark blue block-like single crystals suitable for structural analysis were obtained after 2 weeks. Yield: 65%. IR (KBr, cm^{-1}): 1642, 1537, 1441, 1187, 1091.

■ ASSOCIATED CONTENT

Ⓢ Supporting Information

A crystallographic data file (CIF files) for complexes **1**−**4**. Spectroscopic data, experimental procedures, structural diagrams, and additional magnetic data (Figures S1−S10). DFT calculations details. This material is available free of charge via the Internet at http://pubs.acs.org.

■ AUTHOR INFORMATION

Corresponding Author

*E-mail: kouhz@mail.tsinghua.edu.cn.

Notes

The authors declare no competing financial interest.

■ ACKNOWLEDGMENTS

This work was supported by 973 Program (2013CB933403) and the National Natural Science Foundation of China (Project Nos. 91222104 and 21171103). We gratefully acknowledge the assistance of Tian Zhou in the theoretical study.

REFERENCES

(1) (a) Sato, O. *Acc. Chem. Res.* **2003**, *36*, 692−700. (b) Bai, Y.-L.; Tao, J.; Huang, R.-B.; Zheng, L.-S.; Zheng, S.-L.; Oshida, K.; Einaga, Y. *Chem. Commun.* **2008**, 1753−1755.

(2) Hauser, A. *Top. Curr. Chem.* **2004**, *233*, 49−58.

(3) Olguín, J.; Brooker, S. in: Halcrow, M. A. *Spin-Crossover Materials: Properties and Applications;* John Wiley & Sons: Hoboken, 2013.

(4) (a) Halcrow, M. A. *Polyhedron* **2007**, *26*, 3523−3576. (b) Goodwin, H. A. *Top. Curr. Chem.* **2004**, *234*, 23−47. (c) Krivokapic, I.; Zerara, M.; Daku, M. L.; Vargas, A.; Enachescu, C.; Ambrus, C.; Tregenna-Piggott, P.; Amstutz, N.; Krausz, E.; Hauser, A. *Coord. Chem. Rev.* **2007**, *251*, 364−378. (d) Hayami, S.; Komatsu, Y.; Shimizu, T.; Kamihata, H.; Lee, Y.-H. *Coord. Chem. Rev.* **2011**, *255*, 1981−1990. (e) Gütlich, P.; Hauser, A.; Spiering, H. *Angew. Chem., Int. Ed.* **1994**, *33*, 2024−2054. (f) Zarembowitch, J. *New J. Chem.* **1992**, *16*, 255−267. (g) Murray, K. S.; Eur, J. *Inorg. Chem.* **2008**, 3101−3121. (h) Kilner, C. A.; Halcrow, M. A. *Dalton Trans.* **2010**, *39*, 9008−9012. (i) Harris, C. M.; Lockyer, T. N.; Martin, R. L.; Patil, H. R. H.; Sinn, E.; Stewart, I. M. *Aust. J. Chem.* **1969**, *22*, 2105−2116. (j) Vecchio-Sadus, A. M. *Transition Met. Chem.* **1995**, *20*, 38−45. (k) Cowan, M. G.; Olguín, J.; Narayanaswamy, S.; Tallon, J. L.; Brooker, S. *J. Am. Chem. Soc.* **2012**, *134*, 2892−2894. (l) Beckmann, U.; Brooker, S. *Coord. Chem. Rev.* **2003**, *245*, 17−29. (m) Gass, I. A.; Tewary, S.; Nafady, A.; Chilton, N. F.; Gartshore, C. J.; Asadi, M.; Lupton, D. W.; Moubaraki, B.; Bond, A. M.; Boas, J. F.; Guo, S.-X.; Rajaraman, G.; Murray, K. S. *Inorg. Chem.* **2013**, *52*, 7557−7572. (n) Cook, L. J. K.; Tuna, F.; Halcrow, M. A. *Dalton Trans.* **2013**, *42*, 2254−2265.

(5) (a) Atmani, C.; El Hajj, F.; Benmansour, S.; Marchivie, M.; Triki, S.; Conan, F.; Patinec, V.; Handel, H.; Dupouy, G.; Gómez-García, C. J. *Coord. Chem. Rev.* **2010**, *254*, 1559−1569. (b) Bao, X.; Shepherd, H. J.; Salmon, L.; Molnár, G.; Tong, M.-L.; Bousseksou, A. *Angew. Chem., Int. Ed.* **2013**, *52*, 1198−1202. (c) Chuang, Y.-C.; Liu, C.-T.; Sheu, C.-F.; Ho, W.-L.; Lee, G.-H.; Wang, C.-C.; Wang, Y. *Inorg. Chem.* **2012**, *51*, 4663−4671. (d) Graf, M.; Wolmershäuser, G.; Kelm, H.; Demeschko, S.; Meyer, F.; Krüger, H.-J. *Angew. Chem., Int. Ed.* **2010**, *49*, 950−953.

(6) (a) Lin, J.-B.; Xue, W.; Wang, B.-Y.; Tao, J.; Zhang, W.-X.; Zhang, J.-P.; Chen, X.-M. *Inorg. Chem.* **2012**, *51*, 9423−9430. (b) Bao, X.; Guo, P.-H.; Liu, W.; Tucek, J.; Zhang, W.-X.; Leng, J.-D.; Chen, X.-M.; Gural'skiy, Il'ya; Salmon, L.; Bousseksou, A.; Tong, M.-L. *Chem. Sci.* **2012**, *3*, 1629−1633. (c) Hayami, S.; Hashiguchi, K.; Juhasz, G.; Ohba, M.; Okawa, H.; Maeda, Y.; Kato, K.; Osaka, K.; Takada, M.; Inoue, K. *Inorg. Chem.* **2004**, *43*, 4124−4126.

(7) Clérac, R.; Cotton, F. A.; Daniels, L. M.; Dunbar, K. R.; Kirschbaum, K.; Murillo, C. A.; Pinkerton, A. A.; Schultz, A. J.; Wang, X.-P. *J. Am. Chem. Soc.* **2000**, *122*, 6226−6236.

(8) (a) Bonnet, S.; Siegler, M. A.; Costa, J. S.; Molnár, G.; Bousseksou, A.; Spek, A. L.; Gamez, P.; Reedijk, J. *Chem. Commun.* **2008**, 5619−5621. (b) Nihei, M.; Ui, M.; Yokota, M.; Han, L.; Maeda, A.; Kishida, H.; Okamoto, H.; Oshio, H. *Angew. Chem., Int. Ed.* **2005**, *44*, 6484−6487.

(9) (a) Wang, Y.-T.; Li, S.-T.; Wu, S.-Q.; Cui, A.-L.; Shen, D.-Z.; Kou, H.-Z. *J. Am. Chem. Soc.* **2013**, *135*, 5942−5945. (b) Wu, S.-Q.; Xie, Q.-W.; An, G.-Y.; Chen, X.; Liu, C.-M.; Cui, A.-L.; Kou, H.-Z. *Dalton Trans.* **2013**, *42*, 4369−4372. (c) Hardy, J. G. *Chem. Soc. Rev.* **2013**, *42*, 7881−7899.

(10) (a) Newton, G. N.; Onuki, T.; Shiga, T.; Noguchi, M.; Matsumoto, T.; Mathieson, J. S.; Nihei, M.; Nakano, M.; Cronin, L.; Oshio, H. *Angew. Chem., Int. Ed.* **2011**, *50*, 4844−4848. (b) Schneider, B.; Demeshko, S.; Dechert, S.; Meyer, F. *Angew. Chem., Int. Ed.* **2010**, *49*, 9274−9277.

(11) Plante, J. P.; Jones, P. D.; Powell, D. R.; Glass, T. E. *Chem. Commun.* **2003**, 336−337.

(12) Breuning, E.; Ruben, M.; Lehn, J.-M.; Renz, F.; Garcia, Y.; Ksenofontov, V.; Gütlich, P.; Wegelius, E.; Rissanen, K. *Angew. Chem., Int. Ed.* **2000**, *39*, 2504−2507.

(13) (a) Uppadine, L. H.; Lehn, J.-M. *Angew. Chem., Int. Ed.* **2004**, *43*, 240−243. (b) Stefankiewicz, A. R.; Rogez, G.; Harrowfield, J.; Sobolev, A. N.; Madalan, A.; Huuskonen, J.; Rissanen, K.; Lehn, J.-M. *Dalton Trans.* **2012**, *41*, 13848−13855. (c) Stefankiewicz, A. R.; Lehn, J.-M. *Chem.—Eur. J.* **2009**, *15*, 2500−2503.

(14) (a) Wu, D.-Y.; Sato, O.; Einaga, Y.; Duan, C.-Y. *Angew. Chem., Int. Ed.* **2009**, *48*, 1475−1478. (b) Wei, R.-J.; Huo, Q.; Tao, J.; Huang, R.-B.; Zheng, L.-S. *Angew. Chem., Int. Ed.* **2011**, *50*, 8940−8943.

(15) Brooker, S.; Plieger, P. G.; Moubaraki, B.; Murray, K. S. *Angew. Chem., Int. Ed.* **1999**, *38*, 408−410.

(16) Wang, Y.-T.; Cui, A.-L.; Shen, D.-Z.; Kou, H.-Z. *Polyhedron* **2013**, *52*, 970−975.

(17) (a) Guionneau, P.; Marchivie, M.; Bravic, G.; Letard, J. F.; Chasseau, D. *J. Mater. Chem.* **2002**, *12*, 2546−2551. (b) Rodriguez-Carvajal, J.; Hennion, M.; Moussa, F.; Moudden, A. H.; Pinsard, L.; Revcolevschi, A. *Phys. Rev.* **1998**, *B57*, R3189−R3192.

(18) Uppadine, L. H.; Gisselbrecht, J.-P.; Kyritsakas, N.; Nättinen, K.; Rissanen, K.; Lehn, J.-M. *Chem.—Eur. J.* **2005**, *11*, 2549−2565.

(19) (a) Gaspar, A. B.; Munoz, C. M.; Niel, V.; Real, J. A. *Inorg. Chem.* **2001**, *40*, 9−10. (b) Hogg, R.; Wilkins, R. G. *J. Chem. Soc.* **1962**, 341−350. (c) Judge, J. S.; Baker, W. A. *Inorg. Chim. Acta* **1967**, *1*, 68−72. (d) Kou, H.-Z.; Sato, O. *Inorg. Chem.* **2007**, *46*, 9513−9515.

(20) Lloret, F.; Julve, M.; Cano, J.; Ruiz-García, R.; Pardo, E. *Inorg. Chim. Acta* **2008**, *361*, 3432−3445.

(21) (a) Ruben, M.; Lehn, J.-M.; Vaughan, G. *Chem. Commun.* **2003**, 1338−1339. (b) Kovbasyuk, L.; Pritzkow, H.; Krämer, R. *Eur. J. Inorg. Chem.* **2005**, 894−900. (c) Hanan, G. S.; Volkmer, D.; Schubert, U. S.; Lehn, J.-M.; Baum, G.; Fenske, D. *Angew. Chem., Int. Ed. Engl.* **1997**, *36*, 1842−1844. (d) Waldmann, O.; Hassmann, J.; Müller, P.; Hanan, G. S.; Volkmer, D.; Schubert, U. S.; Lehn, J.-M. *Phys. Rev. Lett.* **1997**, *78*, 3390−3393.

(22) Sheldrick, G. M. SHELXL-97. In *Program for Refinement of Crystal Structures;* University of Göttingen: Germany, 1997.

(23) Spek, A. L. *J. Appl. Crystallogr.* **2003**, *36*, 7−13.

(24) Bushuev, M. B.; Krivopalov, V. P.; Semikolenova, N. V.; Shvedenkov, Yu. G.; Sheludyakova, L. A.; Moskalenko, G. G.; Lavrenova, L. G.; Zakharov, V. A.; Larionov, S. V. *Russ. J. Coord. Chem.* **2007**, *33*, 601−606.